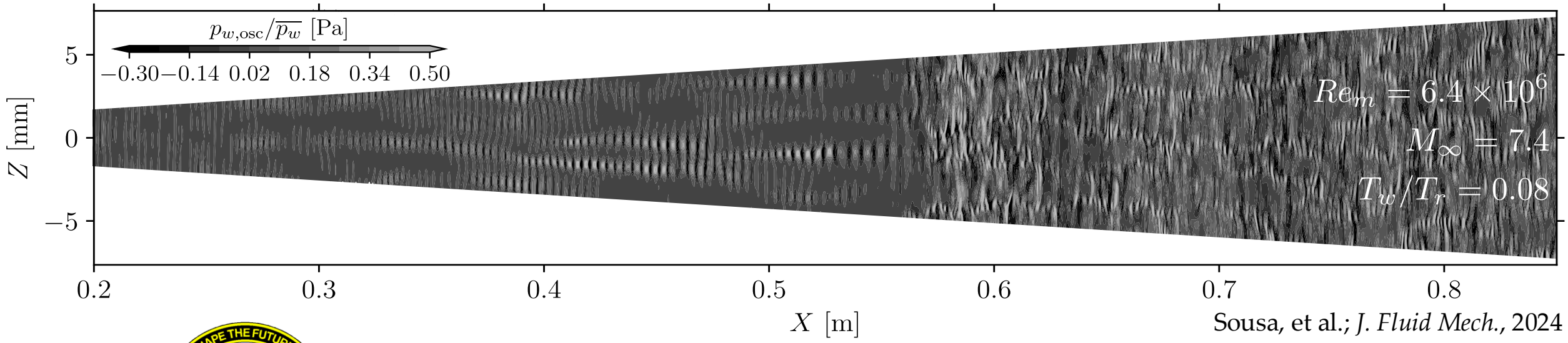
# Second-mode Waves in Hypersonic Transition: Energy Balance, Kinematics and Mechanics

**Indradip Roy, Victor Sousa and Carlo Scalo**

*School of Mechanical Engineering, Purdue University, USA*




Sousa, et al.; *J. Fluid Mech.*, 2024

## Advanced Modeling & Simulation (AMS) Seminar Series

*June 24, 2026*

# Academia, Business and Government



**Engineering Faculty**
**Purdue University**

**Founder of**
**HySonic Technologies**

**Hypersonics SME**
**NSWC Crane**

**DARPA PM**

## Purdue Professor (ME)

- **AFOSR YIP Award:** *Hypersonic Transition Control*
- **ARO YIP Award:** *Large-Scale Vortex Dynamics*
- **ONR YIP Award:** *Hypersonic Turbulence*

## Founder of HySonic Technologies

- **Nov 2017:** $10K from NASA Ames (foundation)
- **SBIR Ph1's:** Navy: (2)x$140K; Army, $190K
- **SBIR Ph2's:** DARPA: $1.8M; Army, $1.31M
- **Joint Venture**: HySonic Aerospace & Defense

HYSONIC TECHNOLOGIES

## Government Engagement

**PI on Internal R&D:**

- *FY'25 ILIR: Basic Research*
- *FY'25 IAR: Applied Research*
- *FY'26 NISE: WFD Hypersonics*

**DARPA PM:**

- *extreme scale fluid mechanics, acoustics, propulsion and computing*

DEFENSE SCIENCES OFFICE

## 5th Grade Graduation ('95)

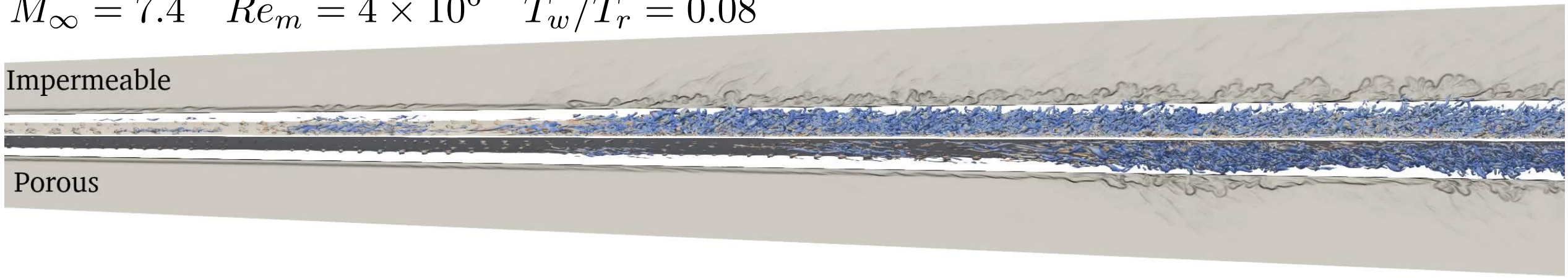



**Allied Joint Force Command (JFC) NATO Base in Naples, Italy**

# Hypersonic Transition Control

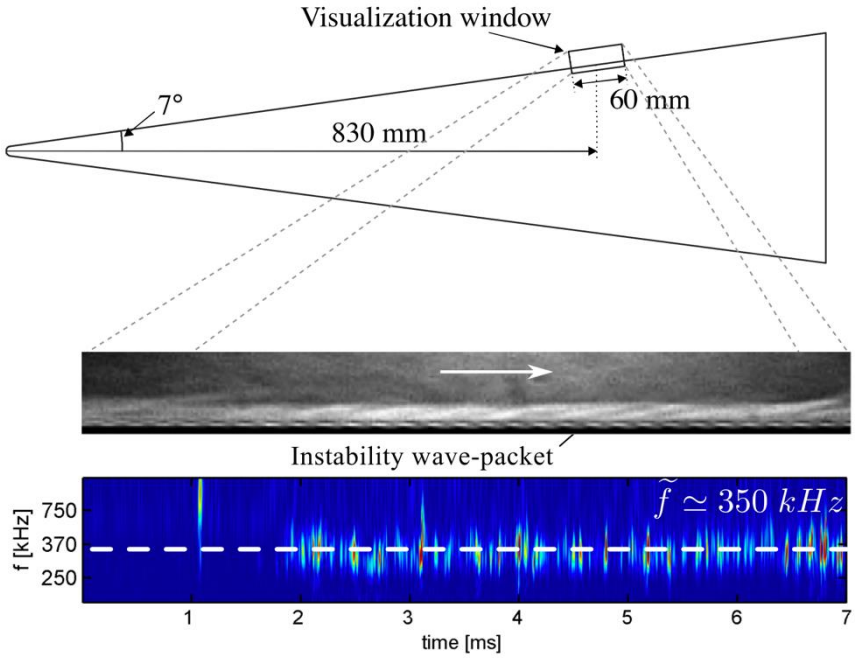
Victor Sousa and Carlo Scalo (2016-2024)

$M_\infty = 7.4 \quad Re_m = 4 \times 10^6 \quad T_w/T_r = 0.08$

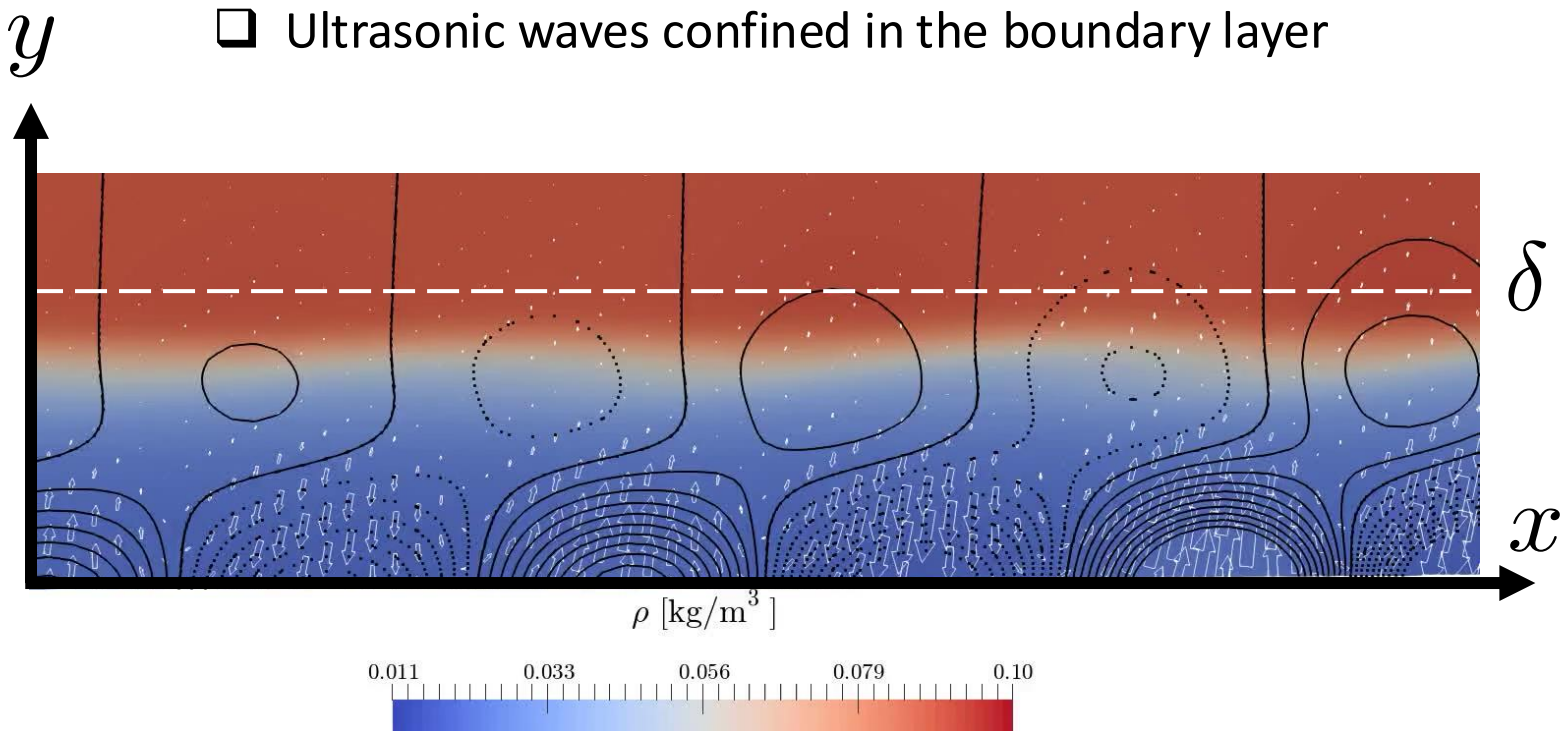


## Second Mode Waves

- Main transition mechanism for hypersonic flows (M>5) in slender geometries



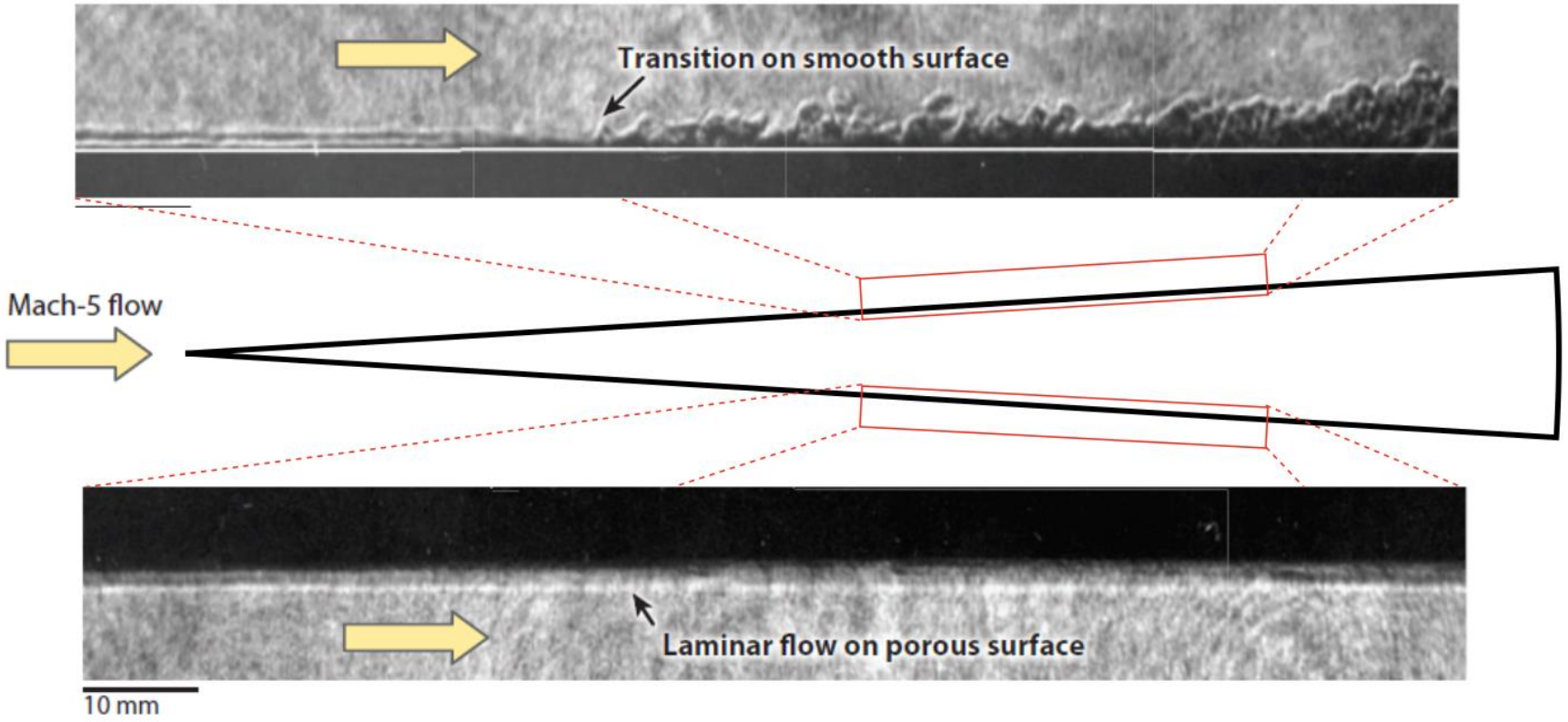

- Ultrasonic waves confined in the boundary layer



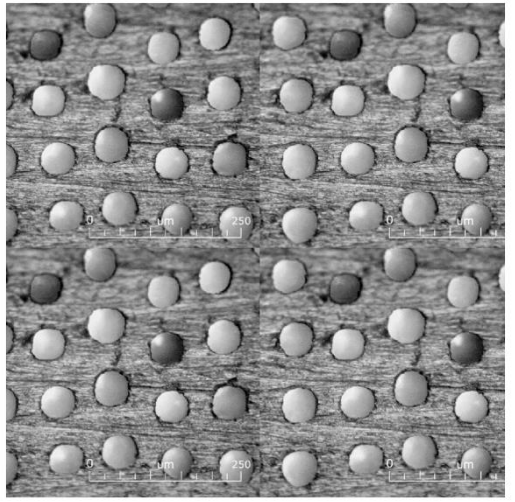

Wagner, PhD Thesis, 2014; Fedorov et al.: AIAA 2001-605.

## Acoustic control of second-mode waves

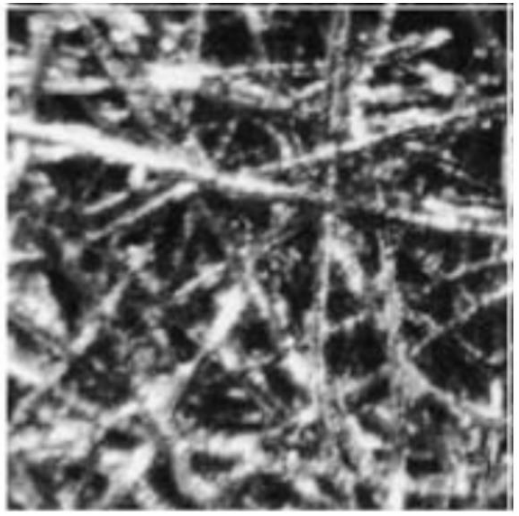
- Can acoustically absorptive materials be used for transition delay?




laser drilled holes



“chicken wire”



Rasheed et al.: AIAA 2002-481. Fedorov et al.: JFM 2003-99.

## Carbon-fiber reinforced ceramics (C/C) by DLR

- Can exhibit porosity while retaining resistance to harsh environments
- Distributed random porosity

**BROAD SPECTRUM OF ACOUSTIC ABSORPTION**

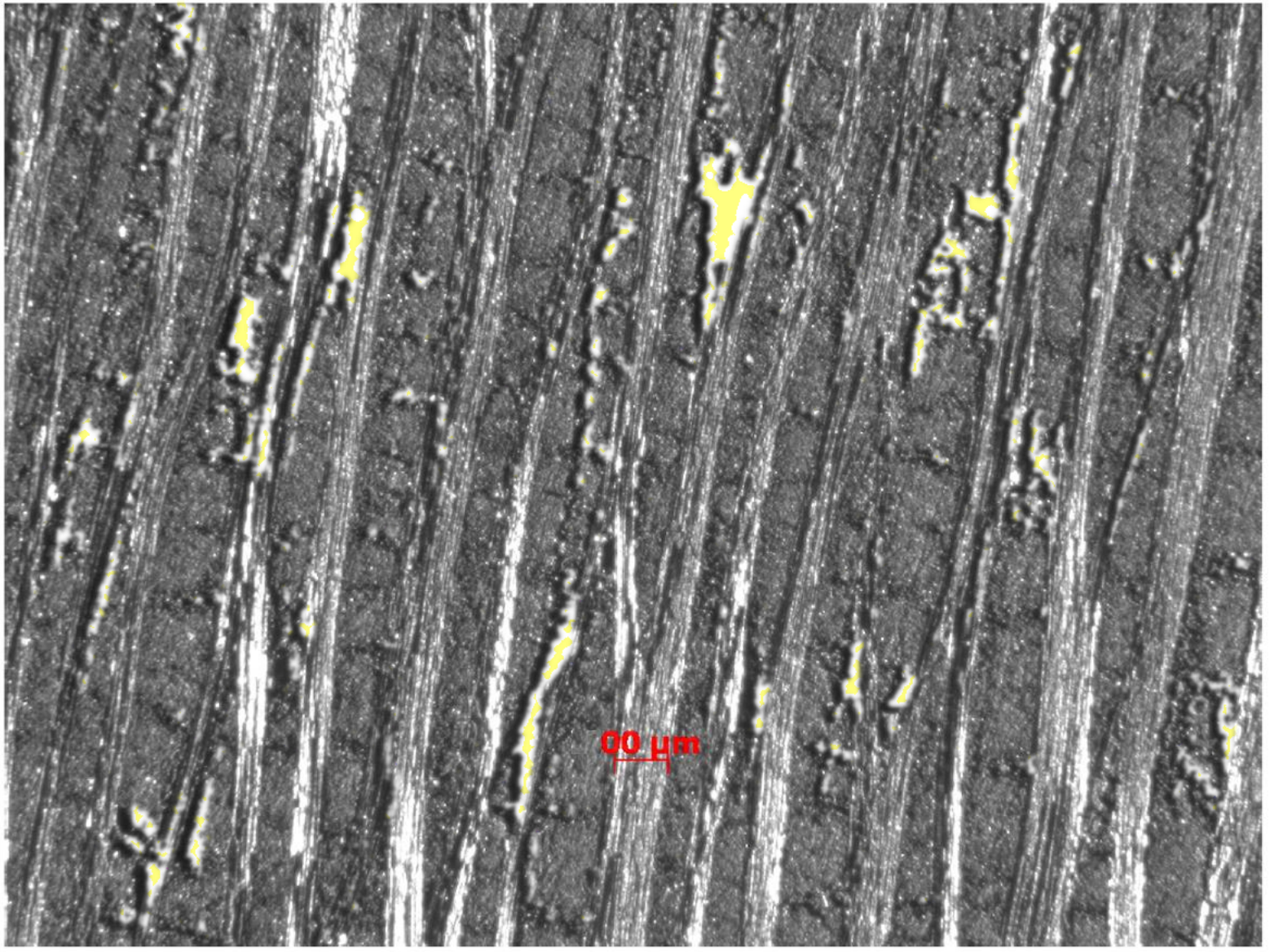
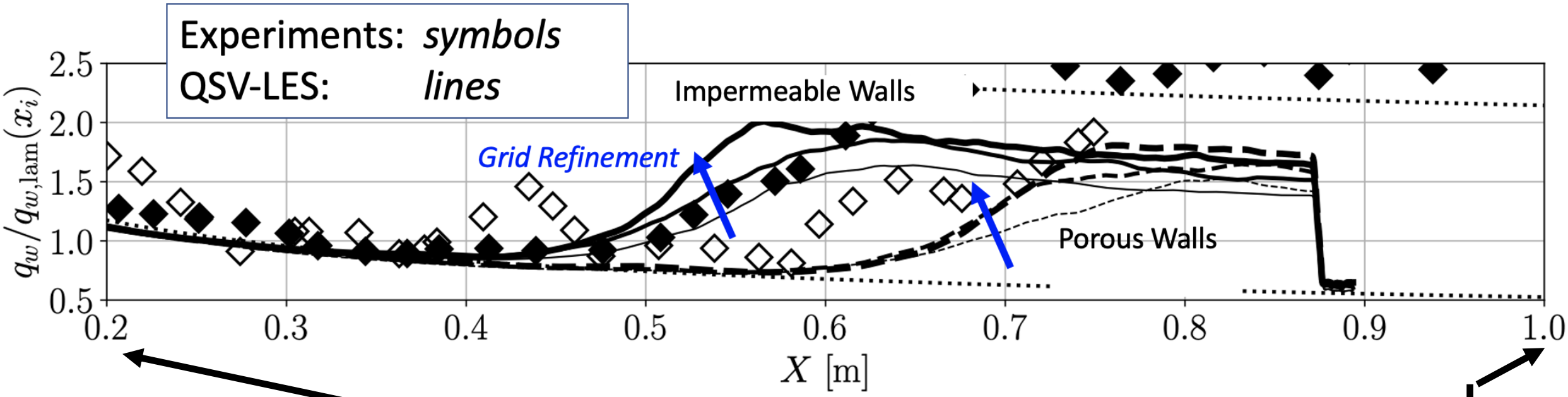
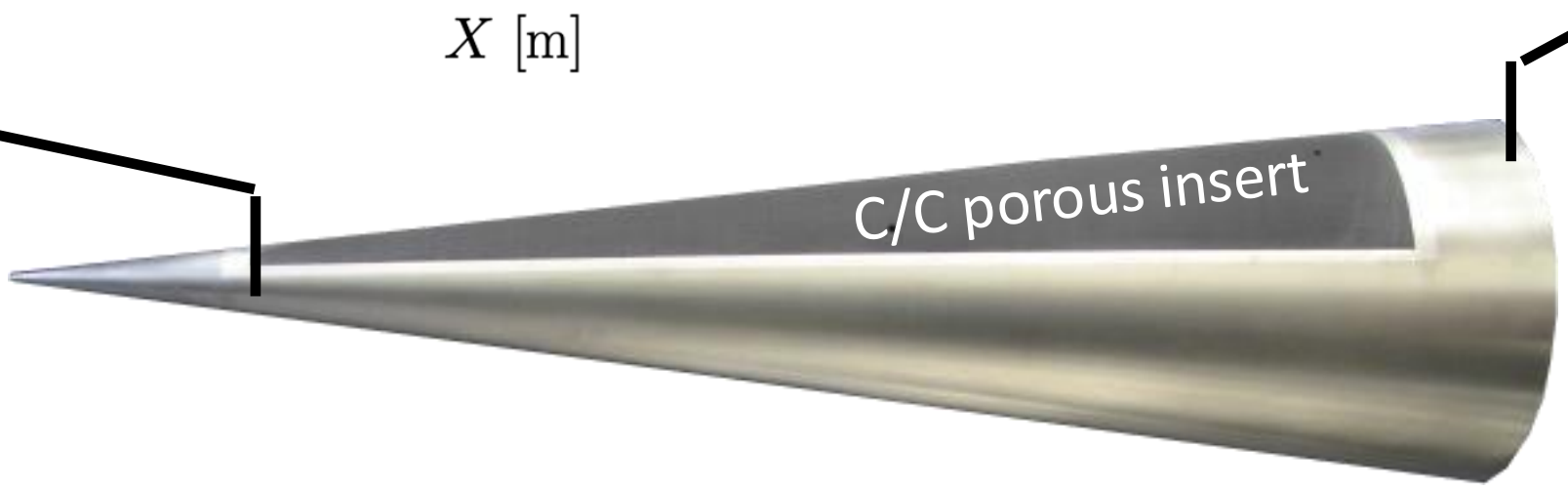



*image courtesy of Dr. Wagner*

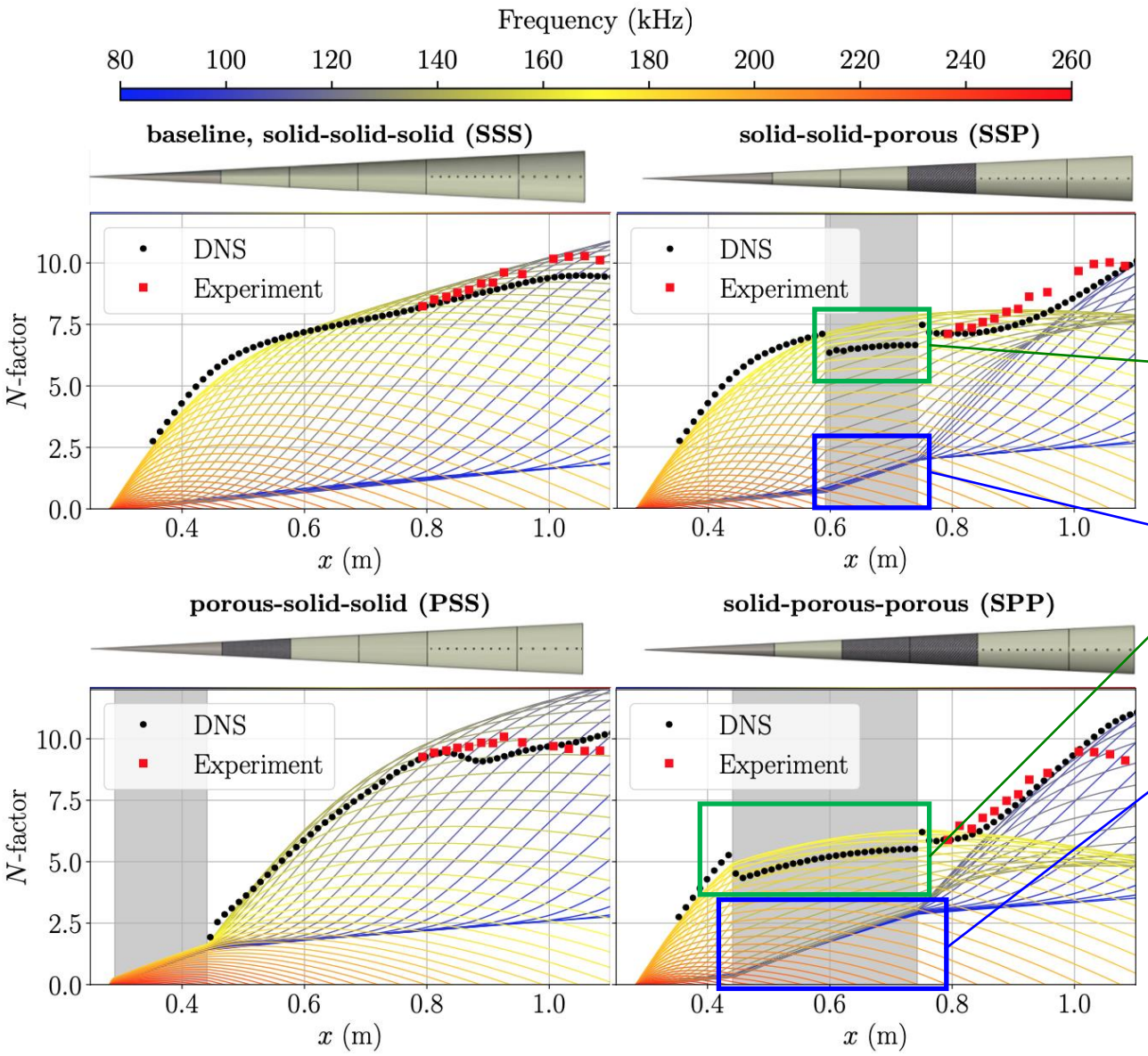
## Reproduce Dr. Wagner's Hypersonic BLT Delay Experiments




**Cone Model with C/C porous insert (Dr. Alex Wagner)**

# Porous Foams




## *N* factor comparisons

- Colored lines – Frequency-by-frequency LST N-factors
- **Black circles** – DNS N-factor predictions
- **Red squares** – BAM6QT N-factor predictions

DNS shows a clear drop in second-mode growth over the foams

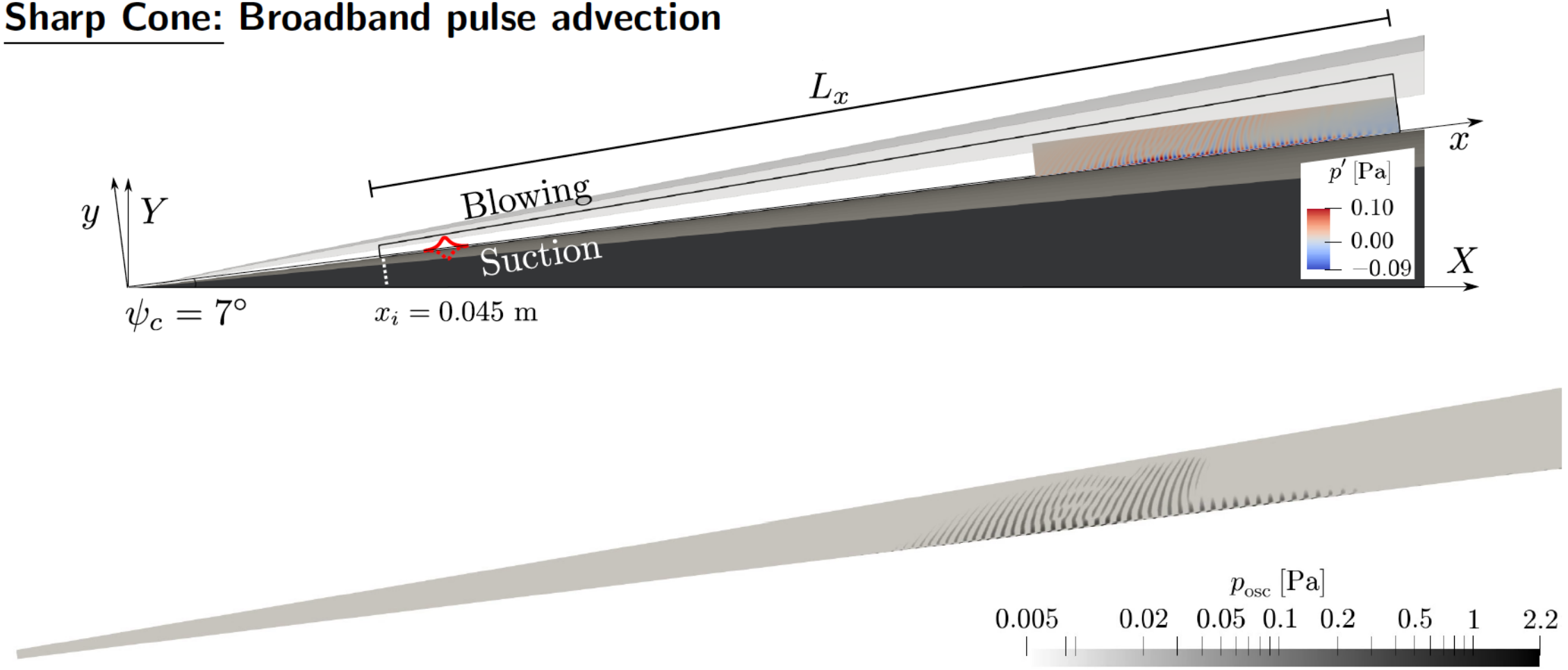
Lower bracket of frequencies are amplified more at the foam

The amplified low frequencies dominate the second-mode wave packet N-factor later downstream

Miller, S., Roy, I., *et al.*, 2026. Hypersonic Boundary Layer Transition Control Over a 3° Half-Angle Sharp Cone via Distributed Porosity. *J. Fluid Mech, 1032, A50*

# Pulsed Calculation

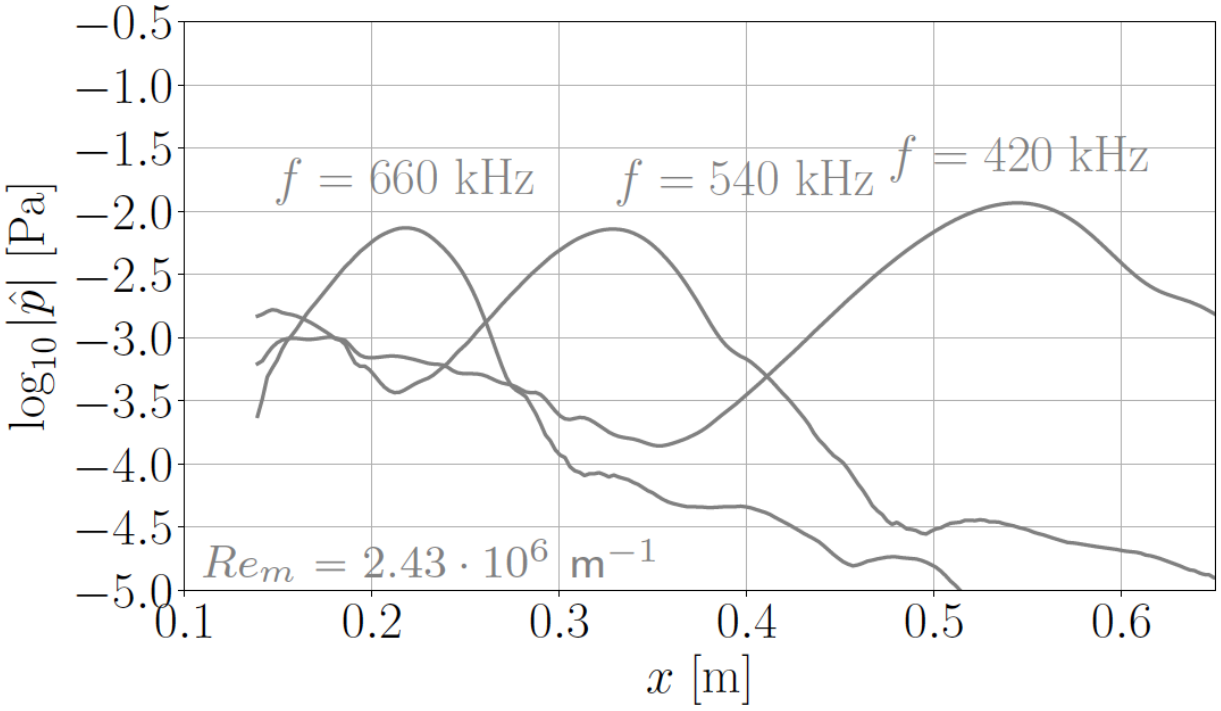
## Sharp Cone: Broadband pulse advection

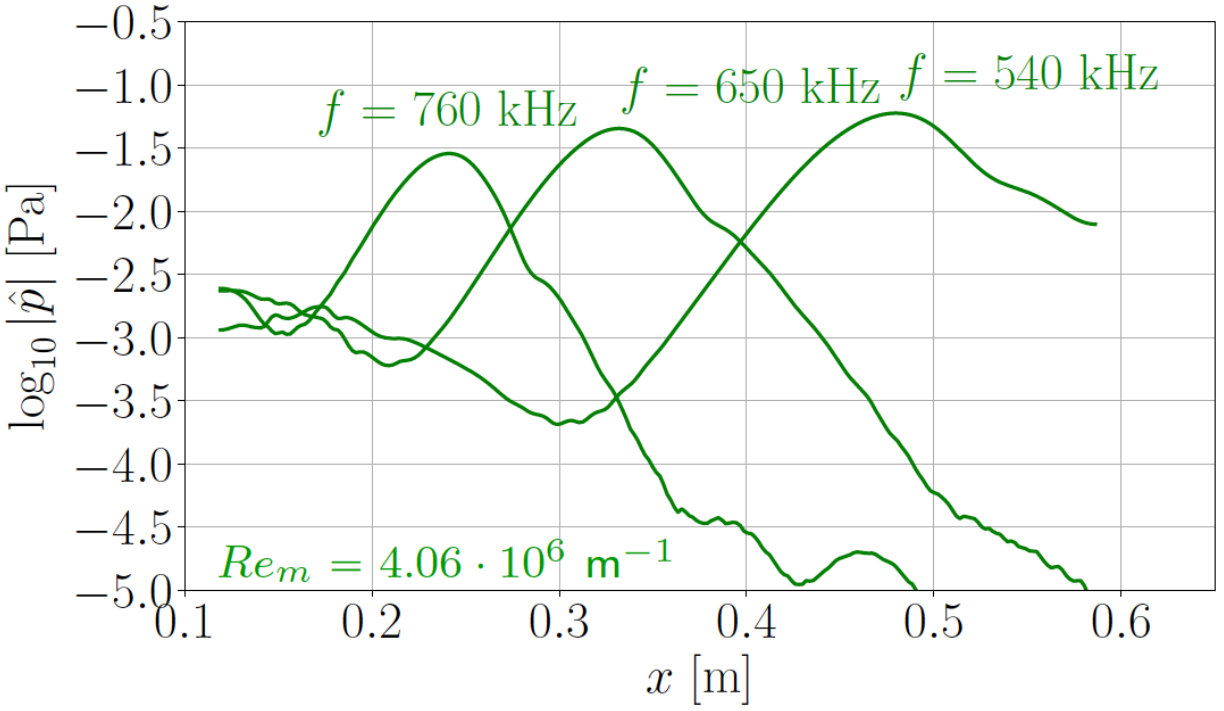



Sousa, Patel, Chapelier, Wartemann, Wagner, and Scalo, *Numerical Investigation of Second Mode Attenuation over Carbon/Carbon Surfaces on a Sharp Slender Cone*, **Journal of Spacecraft and Rockets**, 2019, Vol. 56, No. 2, pp. 319-332

## Sharp Cone Results

- Impermeable Wall 'DNS' (—)



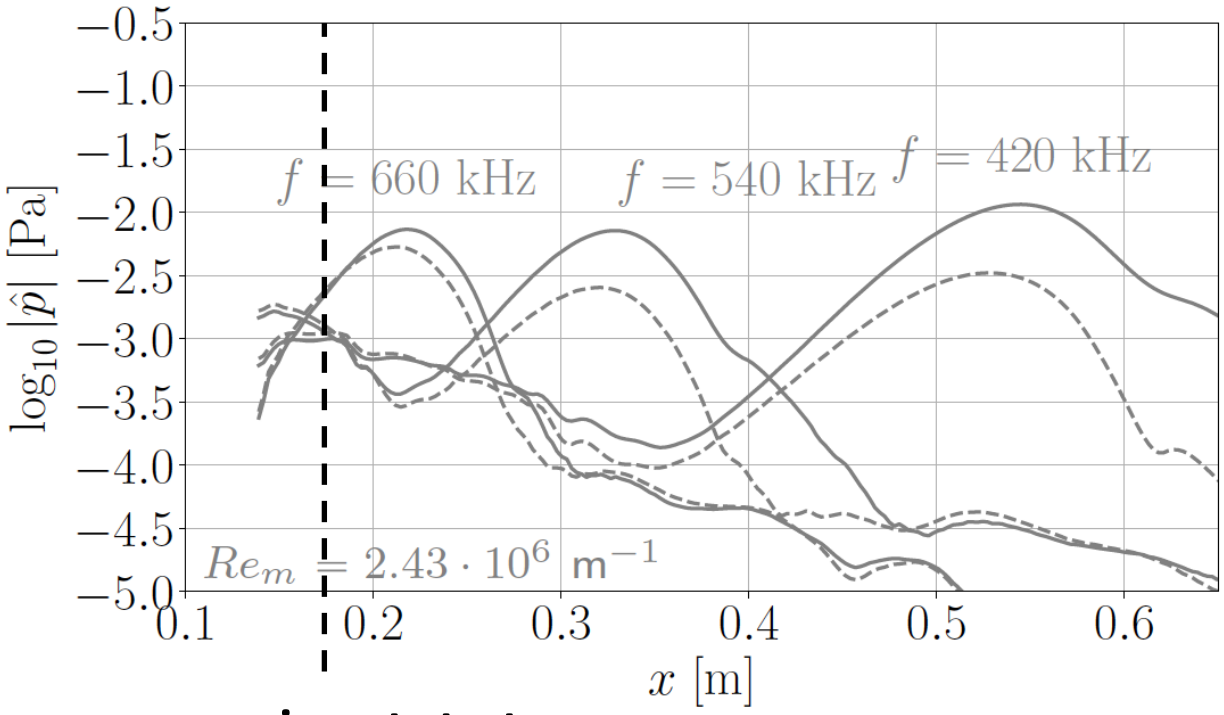




Sousa, Patel, Chapelier, Wartemann, Wagner, and Scalo, *Numerical Investigation of Second Mode Attenuation over Carbon/Carbon Surfaces on a Sharp Slender Cone*, **Journal of Spacecraft and Rockets**, 2019, Vol. 56, No. 2, pp. 319-332

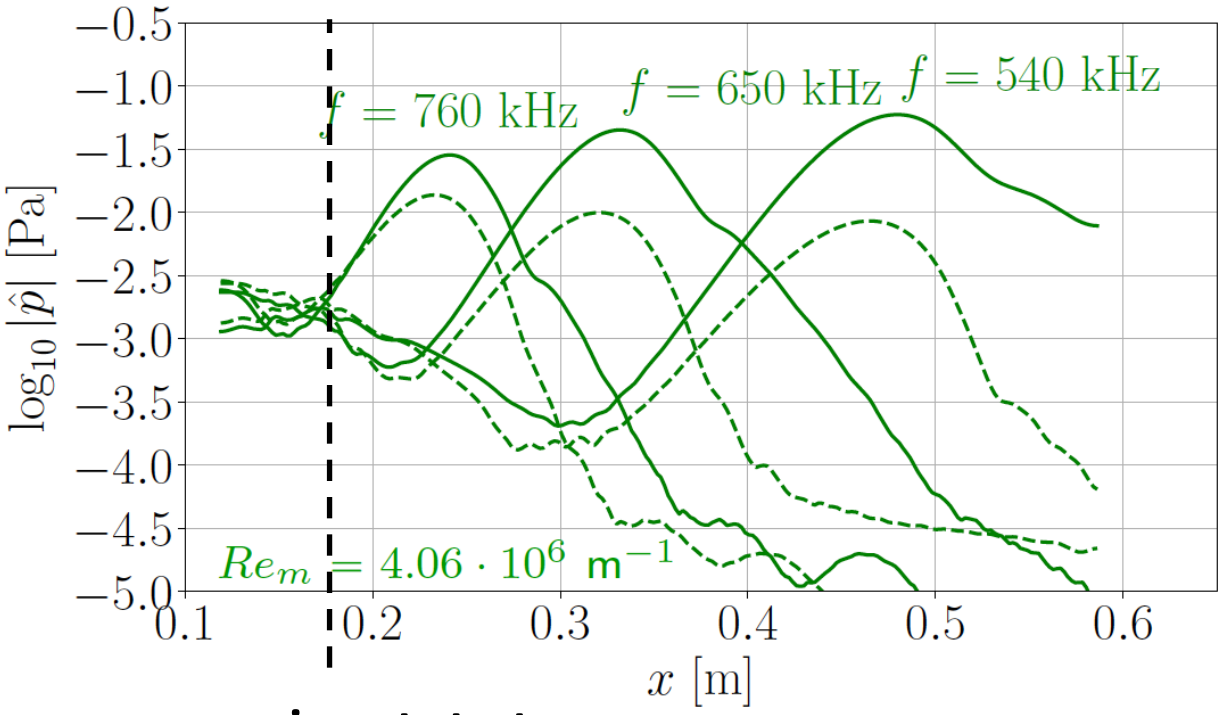
Sousa and Scalo, *A unified Quasi-Spectral Viscosity (QSV) approach to shock capturing and large-eddy simulation*, **J. Comput. Phys.,** 2022, Vol 459, 1111139

## Sharp Cone Results

- Impermeable Wall 'DNS' (—)  Porous Walls w/ TDIBC (- - -)



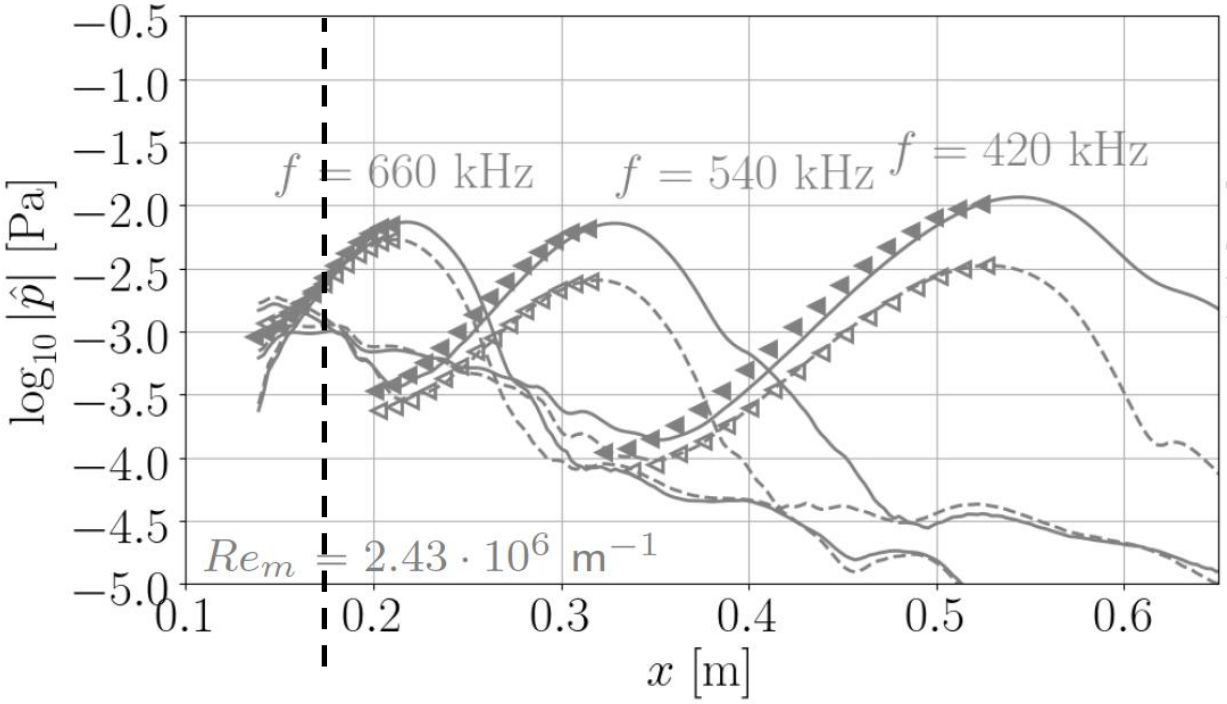

**porous insert start**
**X=0.182 m**



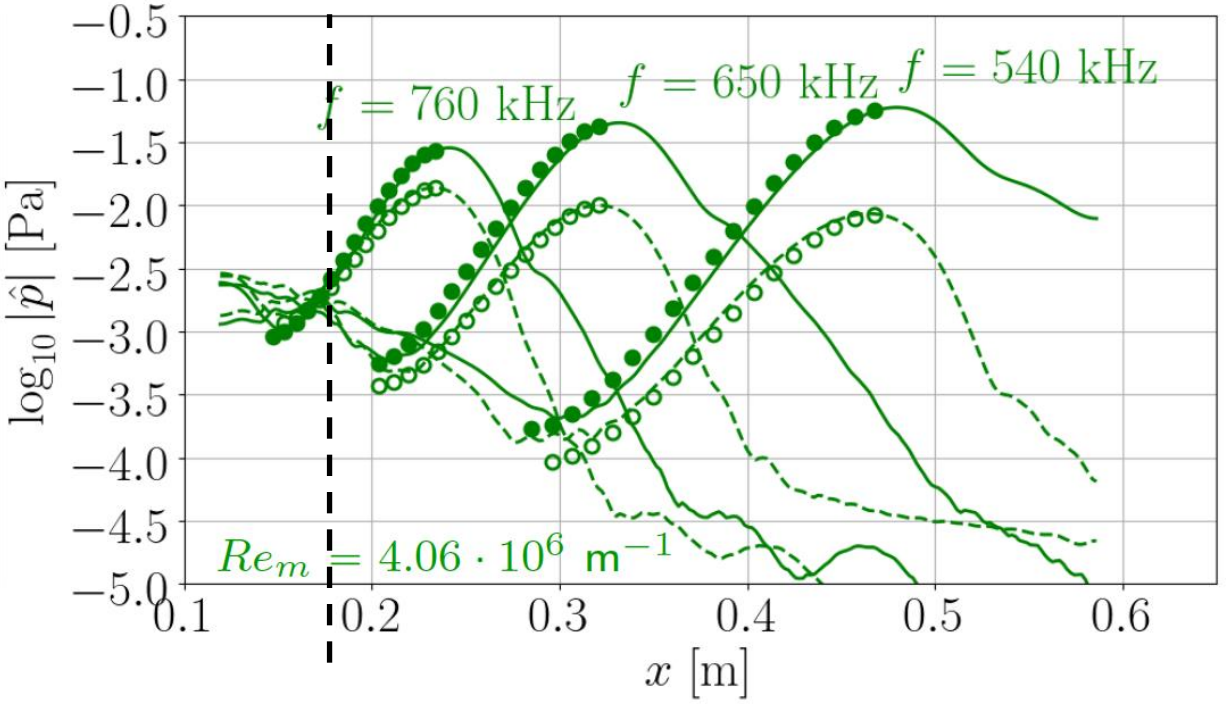

**porous insert start**
**X=0.182 m**

## Sharp Cone Results

- Impermeable Wall 'DNS' (—)  Porous Walls w/ TDIBC (- - -)  Linear-Stability (Symbols)




**porous insert start**
**X=0.182 m**

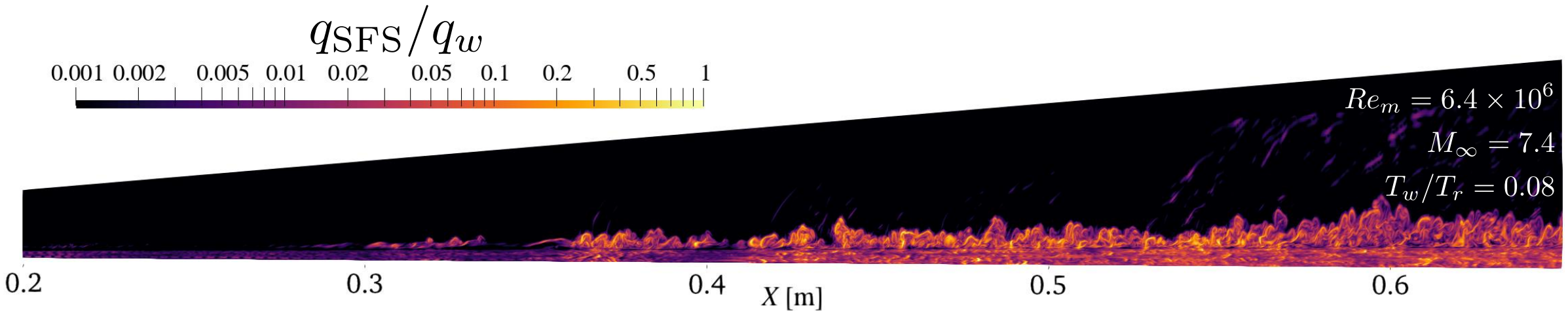



**porous insert start**
**X=0.182 m**

IMPORTANT TWIST: Navier-Stokes calculations come from new dynamic LES model called QSV

# Sub-Filter Scale Closure: QSV-LES

| Color/Symbol | $Re_m$ [1/m] | $M_\infty$ [−] | $p_\infty$ [Pa] | $T_\infty$ [K] | $\rho_\infty$ [kg/m$^3$] |
|---|---|---|---|---|---|
| ★ | $1.46 \cdot 10^6$ | 7.3 | 789 | 267 | 0.0102 |
| ◀ | $2.43 \cdot 10^6$ | 7.4 | 1453 | 285 | 0.0177 |
| ● | $4.06 \cdot 10^6$ | 7.4 | 2129 | 268 | 0.0276 |
| ◆ | $6.40 \cdot 10^6$ | 7.4 | 3083 | 248 | 0.0432 |

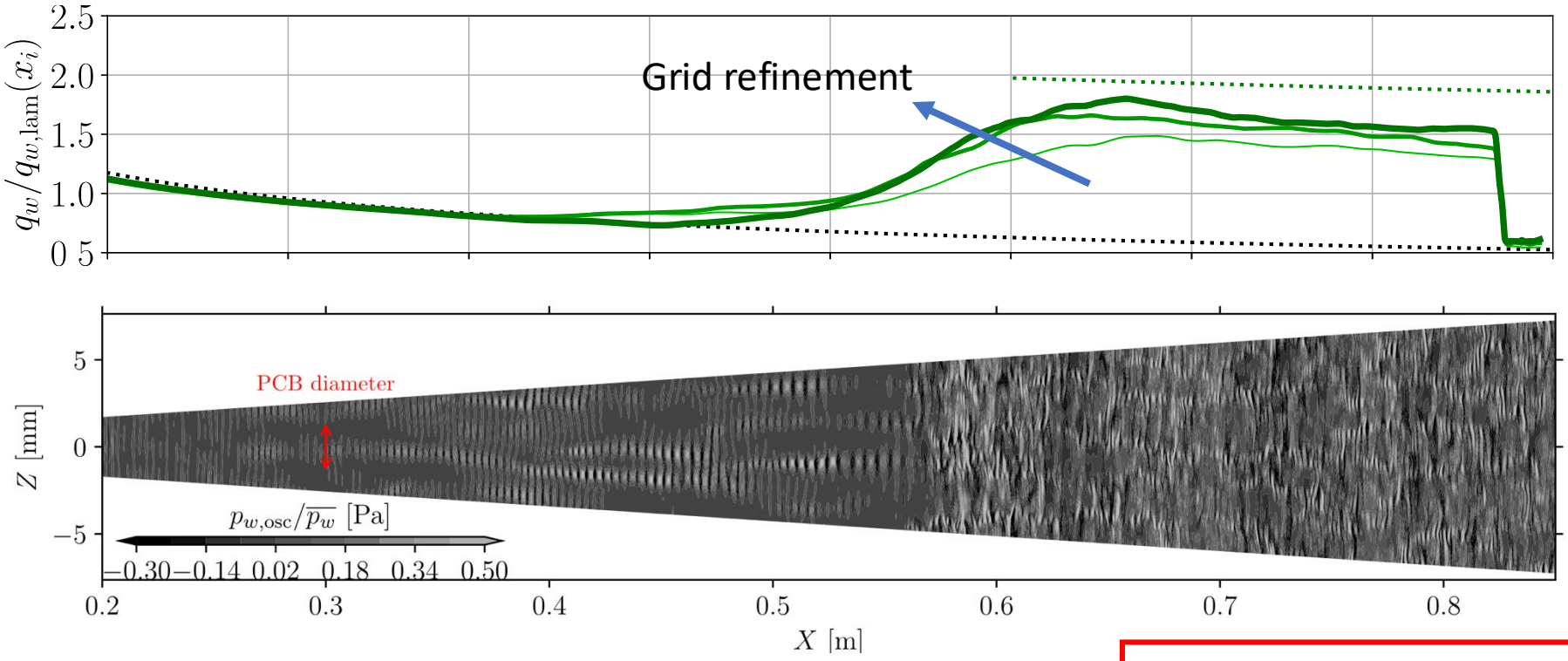




Victor Sousa, A. Wagner, V. Wartemann, Carlo Scalo, "Dynamic Large-Eddy Simulation of Hypersonic Boundary Layer Transition Delay Over Wall-Impedance", *J. Fluid. Mech,* 2024
Victor Sousa and Carlo Scalo, "A unified Quasi-Spectral Viscosity (QSV) approach to shock capturing and large-eddy simulation", *J. Comput. Phys.*, 2022
Victor Sousa and Carlo Scalo, "A Legendre spectral viscosity (LSV) method applied to shock capturing for high-order flux-reconstruction schemes", *J. Comput. Phys.*, 2022

# Sub-Filter Scale Closure: QSV-LES

- LES closure with residual filter sensing of high-wavenumber energy




| Color/Symbol | $Re_m$ [1/m] | $M_\infty$ [−] | $p_\infty$ [Pa] | $T_\infty$ [K] | $\rho_\infty$ [kg/m$^3$] |
|---|---|---|---|---|---|
| ★ | $1.46 \cdot 10^6$ | 7.3 | 789 | 267 | 0.0102 |
| ◀ | $2.43 \cdot 10^6$ | 7.4 | 1453 | 285 | 0.0177 |
| ● | $4.06 \cdot 10^6$ | 7.4 | 2129 | 268 | 0.0276 |
| ◆ | $6.40 \cdot 10^6$ | 7.4 | 3083 | 248 | 0.0432 |

Victor Sousa, Alex Wagner, Viola Wartemann, Carlo Scalo, "Dynamic Large-Eddy Simulation of Hypersonic Boundary Layer Transition Delay Over Wall-Impedance", *J. Fluid. Mechanics,* 2024

Victor Sousa and Carlo Scalo, "A unified Quasi-Spectral Viscosity (QSV) approach to shock capturing and large-eddy simulation", *J. Comput. Phys.*, 2022

Victor Sousa and Carlo Scalo, "A Legendre spectral viscosity (LSV) method applied to shock capturing for high-order flux-reconstruction schemes", *J. Comput. Phys.*, 2022

$$\tau_{mn} = -C_{\tau_{mn}} \frac{1}{2} \left( \mathcal{D}_{mn} \frac{\partial u_m}{\partial x_n} + \mathcal{D}_{nm} \frac{\partial u_n}{\partial x_m} \right)$$

$$\mathcal{D}_{mn} = \upsilon_m(\check{u}_n)\ell_n$$

$$\upsilon_m(\check{u}_n) = \sqrt{\frac{2E^m_{k_c}(\check{u}_n)}{\overline{\Delta}_m}} \rightarrow \text{Velocity scale}$$

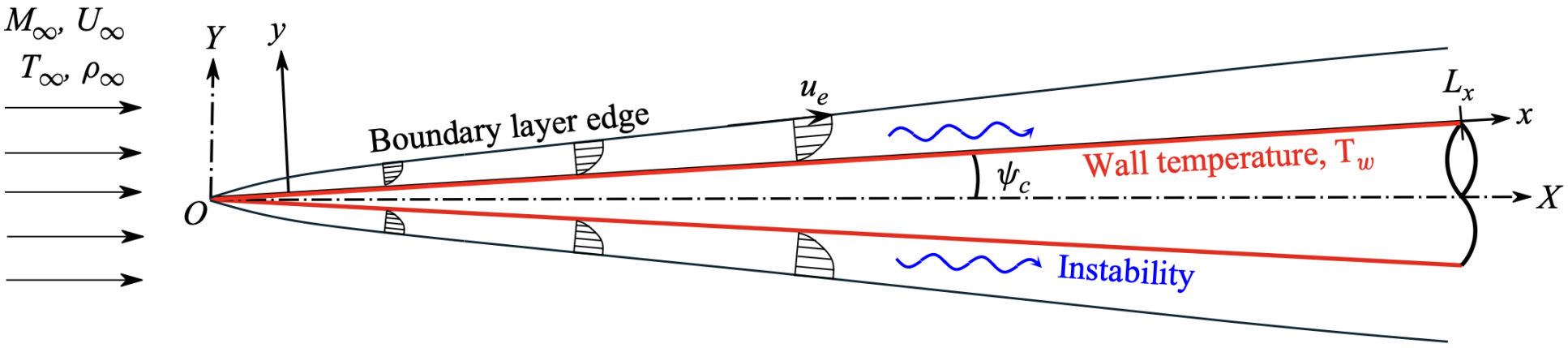
$$\ell_n = \overline{\Delta}_n \rightarrow \text{Length scale}$$

$$\frac{\partial \ddot{u}_m}{\partial x_n} = \frac{\partial \check{u}_m}{\partial x_n} * \left(1 - \tilde{G}_{\mathrm{qsv}}\right)$$

$$\frac{\partial \ddot{T}}{\partial x_n} = \frac{\partial \check{T}}{\partial x_n} * \left(1 - \tilde{G}_{\mathrm{qsv}}\right)$$

# Fundamental Structure of Second-Mode Waves

Indradip Roy and Carlo Scalo (2022-2026)

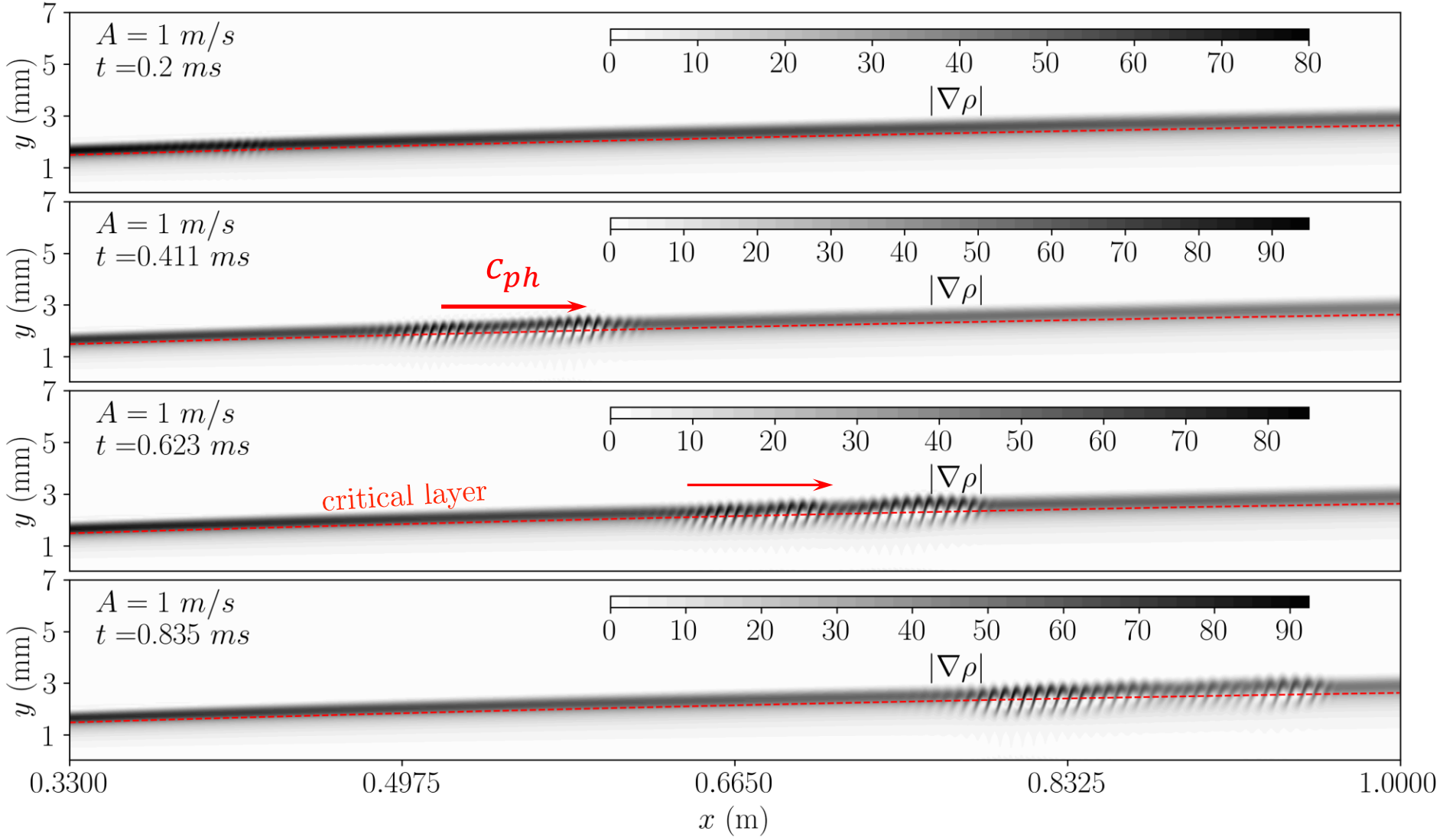



| $\Theta = T_w/T_{ad}$ | $T_w$ [K] |
|---|---|
| 0.25 | 85.362 |
| 0.50 | 170.724 |
| 0.75 | 256.086 |
| 1.00 | 341.448 |
| 1.25 | 426.810 |
| 1.50 | 512.172 |
| 1.75 | 597.534 |

| $M_\infty$ | $Re_\infty$ (1 m$^{-1}$) | $p_\infty$ ($Pa$) | $T_\infty$ ($K$) | $\rho_\infty$ (kg m$^{-3}$) | $U_\infty$ (m s$^{-1}$) | $u_e$ (m s$^{-1}$) | $\mu_\infty$ (Pa s) |
|---|---|---|---|---|---|---|---|
| 6.00 | $11.3 \times 10^6$ | 600.0 | 50.23 | 0.0429 | 852.5567 | 836.55 | $3.2311 \times 10^{-6}$ |

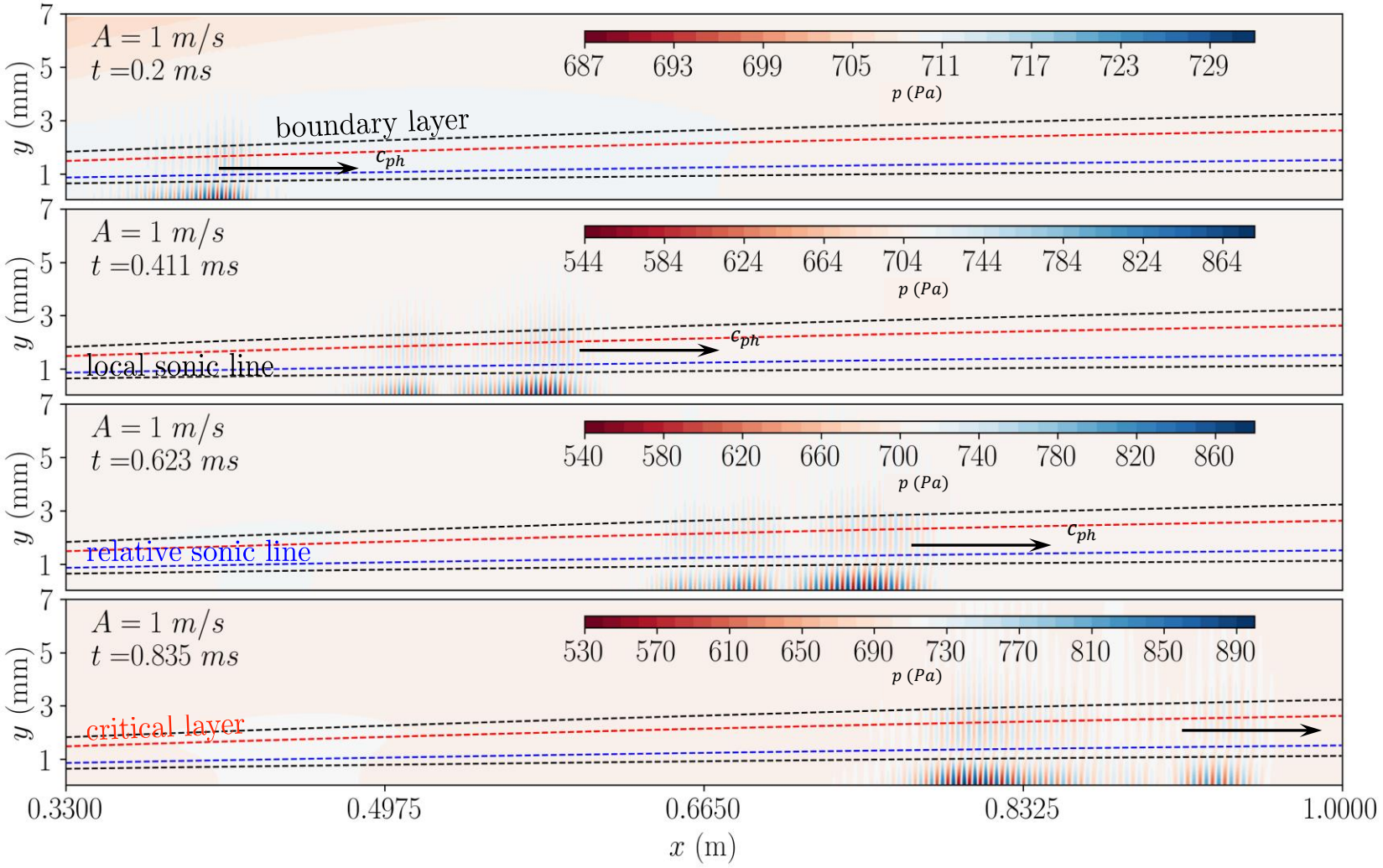
# Second Mode Waves

- "rope-wave" structures occur at the critical layer – only visible at high amplitudes



# Double-deck Structure

- Second modes trap **(a small amount of)** acoustic energy underneath the sonic line
- As the BL and sonic line height increases downstream, second mode frequency decreases:




- Boundary layer $\delta_{\mathrm{BL}}$(99%)
- Critical layer : $\bar{M}(y) = 0$
- *Inflection line* : $(\rho u_0{}')' = 0$
  *** will be shown later*
- Sonic line : $M(y) = 1$
- Relative sonic line : $\bar{M}(y) = {(u_0(y) - c_{ph})}/{a(y)} = -1$

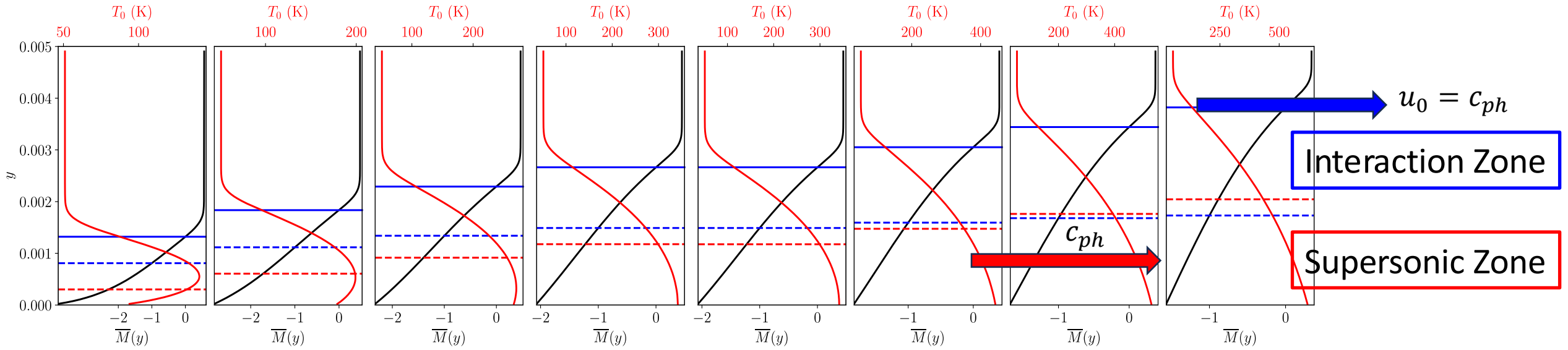
# “Heights” governing second-mode dynamics

| Color | — — | — — | ——— | ——— |
|---|---|---|---|---|
| Label | $y_s$ | $y_r$ | $y_c$ | $BL$ |
| Name | sonic line | relative sonic line | critical layer | boundary layer |
| $u_0(y) =$ | $c_0(y_s)$ | $c_{ph} - c_0(y_r)$ | $c_{ph}$ | $0.999U_e$ |

DNS simulations performed with the cone surface isothermally maintained at different temperatures

| $\Theta = T_w/T_{ad}$ | $T_w$ [K] |
|---|---|
| 0.25 | 85.362 |
| 0.50 | 170.724 |
| 0.75 | 256.086 |
| 1.00 | 341.448 |
| 1.25 | 426.810 |
| 1.50 | 512.172 |
| 1.75 | 597.534 |

increasing wall temperature

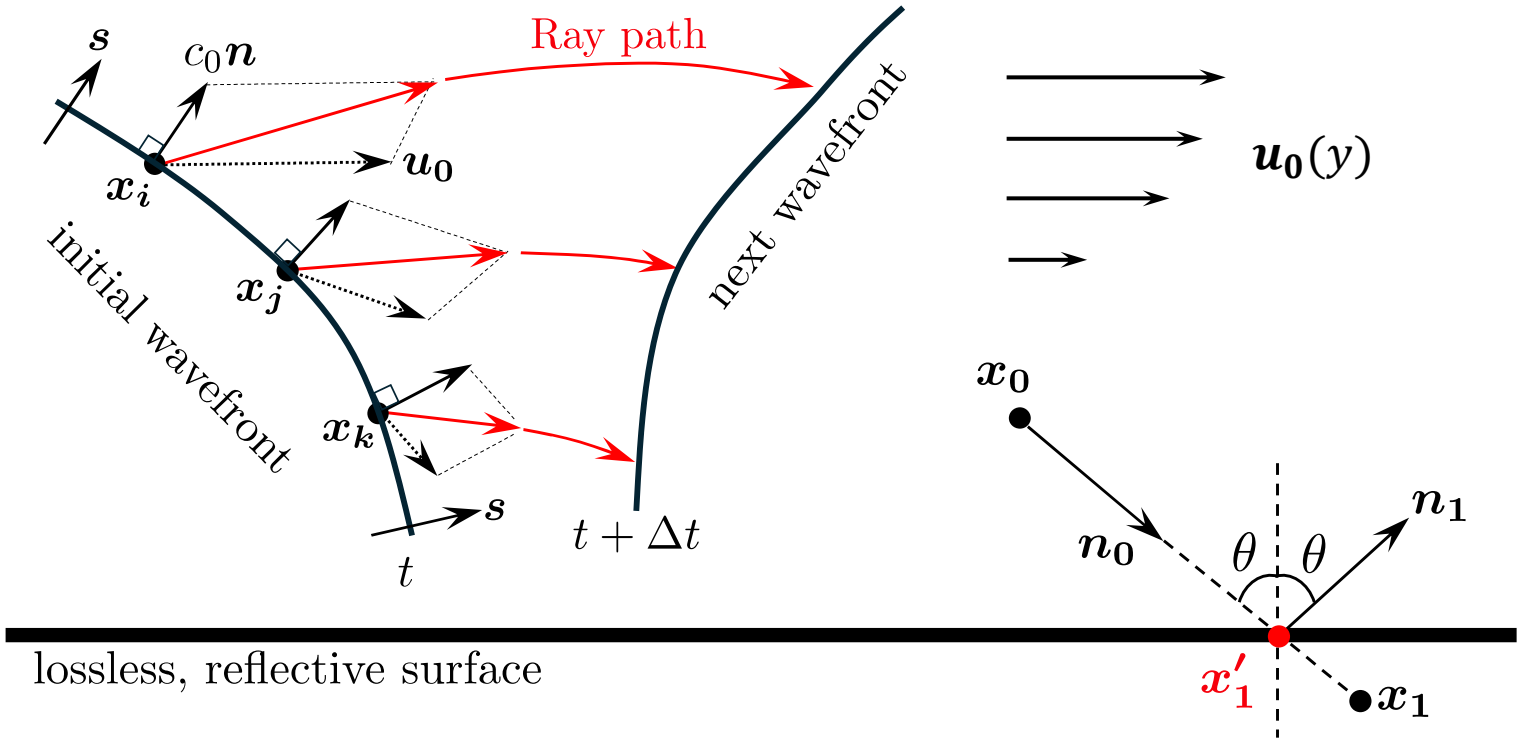


# Kinematics of ~~second mode~~ of acoustic rays

## Wavefront tracking of acoustic rays

Required values:
Mean flow velocity
Mean sound speed

Any ODE solving method can be used to solve this. Used fourth-order Runge-Kutta here

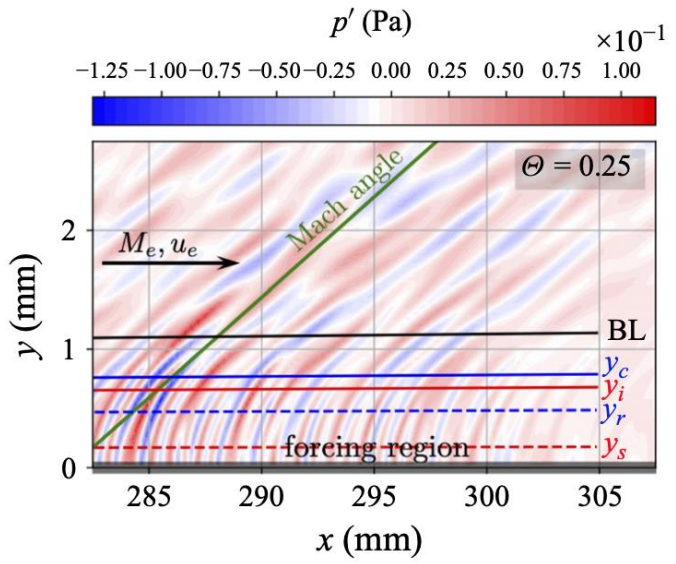


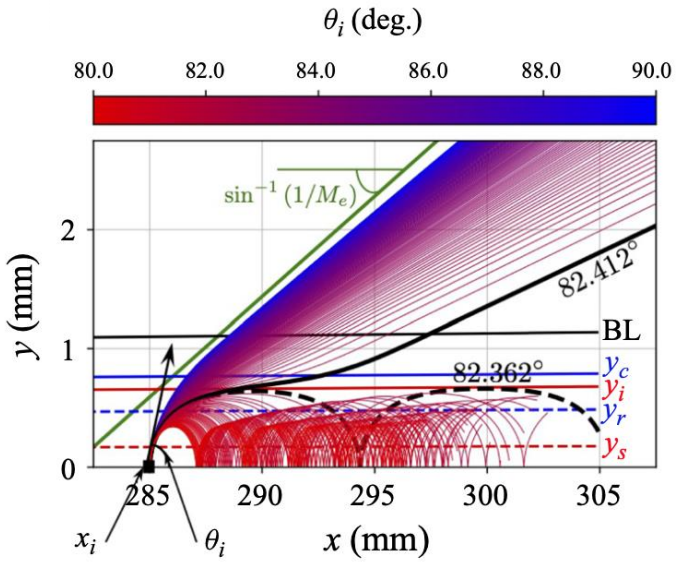

$$\frac{d\boldsymbol{x}}{dt} = \frac{c_0^2 \boldsymbol{s}}{1 - \boldsymbol{u_0} \cdot \boldsymbol{s}} + \boldsymbol{u_0}$$

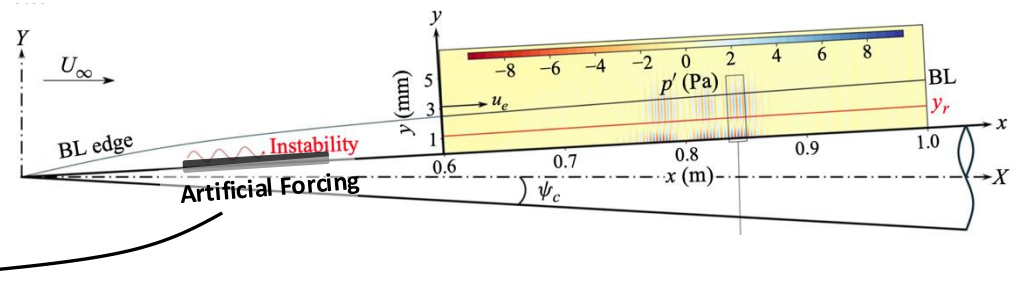
$$\frac{d\boldsymbol{s}}{dt} = -\frac{1 - \boldsymbol{u_0} \cdot \boldsymbol{s}}{c_0} \nabla c_0 - \boldsymbol{s} \times (\nabla \times \boldsymbol{u_0}) - (\boldsymbol{s} \cdot \nabla) \boldsymbol{u_0}$$

# Formation of Second-mode Waves

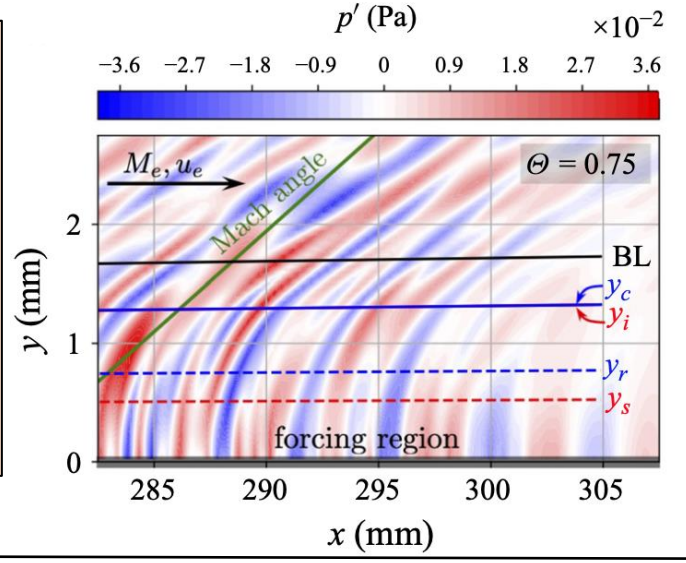
Cold wall, $T_{wall}/T_{ad} = 0.25$

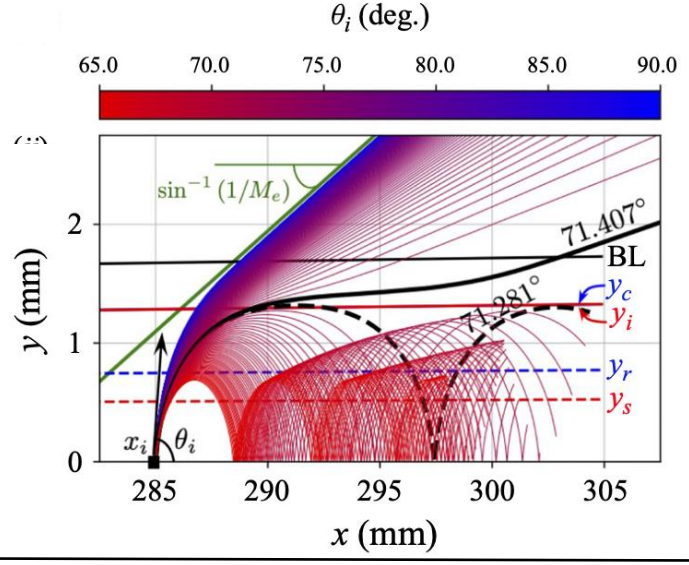



Hot wall, $T_{wall}/T_{ad} = 0.75$



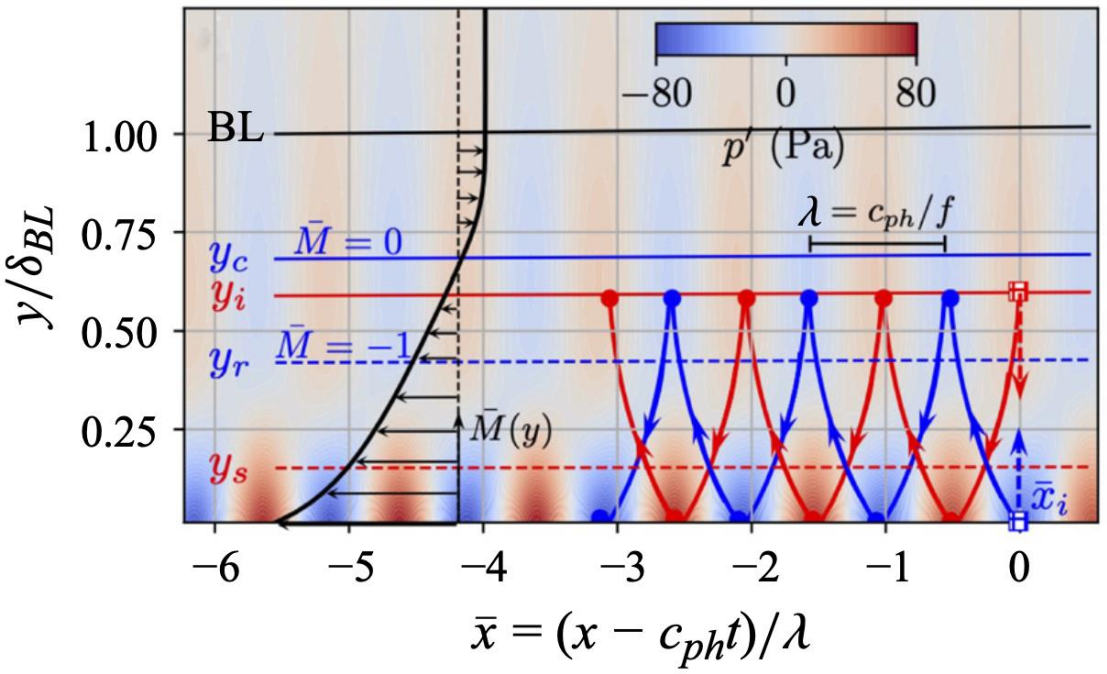

Rays are trapped below the **generalized inflection line** where $\frac{\partial}{\partial y}\left(\rho_0 \frac{\partial u_0}{\partial y}\right) = 0$, *irrespective of the wall temperature*

For colder walls, critical trapping angle is higher => more percentage of rays are trapped

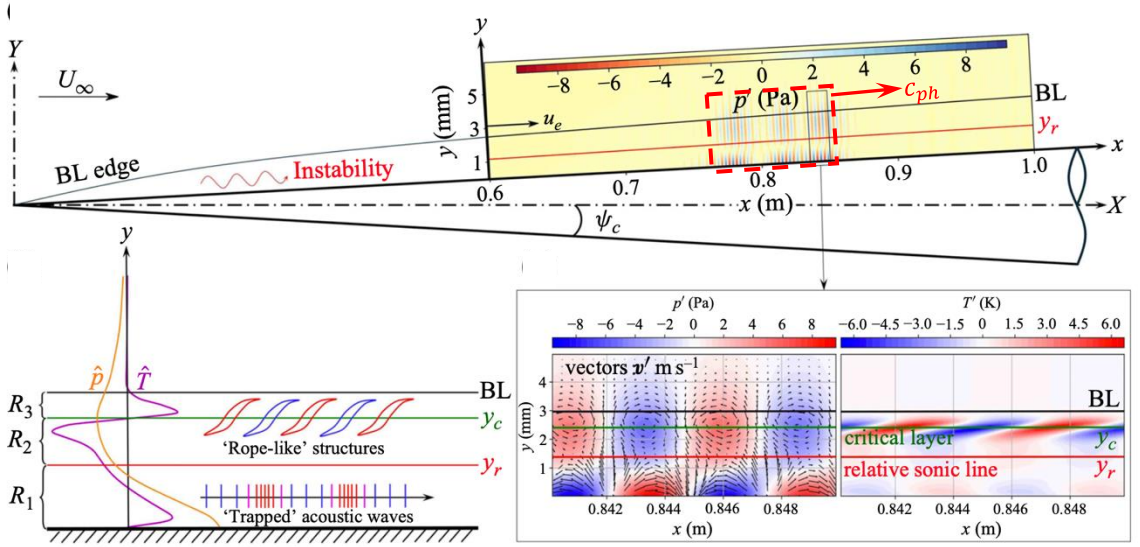
Roy, I. and Scalo, C., 2026. Wall-temperature effects on second-mode kinematics and mechanics. *J. Fluid Mech*, *1027*, p.A7.

# Ray acoustics in moving frame

**Solving ray acoustics in the convective frame attached to the second modes**




$c_{ph}$




- The second modes convect nearly at a constant speed $c_{ph} \sim 0.9u_e$.
- Rays emitted from a pressure minima (blue) and pressure maxima (red) reach the corresponding extrema.
- This simultaneous reflection occurs between the **wall** and **inflection line**, indicating an acoustic standing wave formation

---


Roy, I. and Scalo, C., 2026. Wall-temperature effects on second-mode kinematics and mechanics. *J. Fluid Mech*, *1027*, p.A7.

# Defining the Disturbance Energy

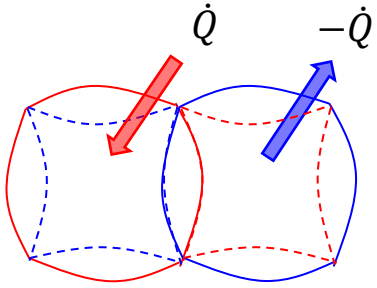
## What is the energy budget of the second-mode waves?

A conservation equation for second-order disturbance energy, $E_2$

$$E_2 = E_t + E_k + E_a = \underbrace{\frac{1}{2}\frac{\rho_0 T_0}{C_p} s'^2}_{i} + \underbrace{\rho' u_{0i} u_i'}_{ii} + \underbrace{\frac{1}{2}\rho_0 u_i'^2}_{iii} + \underbrace{\frac{1}{2}\frac{p'^2}{\gamma p_0}}_{iv}$$

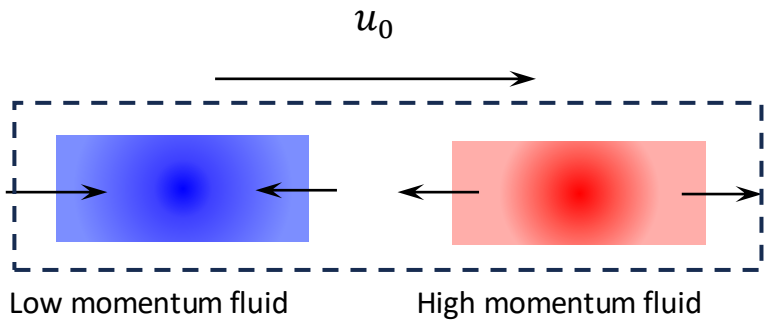
### Thermal energy, term $i$

Energy change due to heat addition in the absence of expansion/compression work



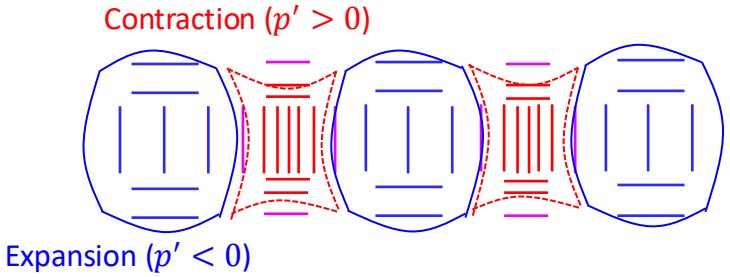

### Kinetic energy , term $ii + iii$

Kinetic energy of the perturbation accounting for momentum fluctuations convected by the base flow



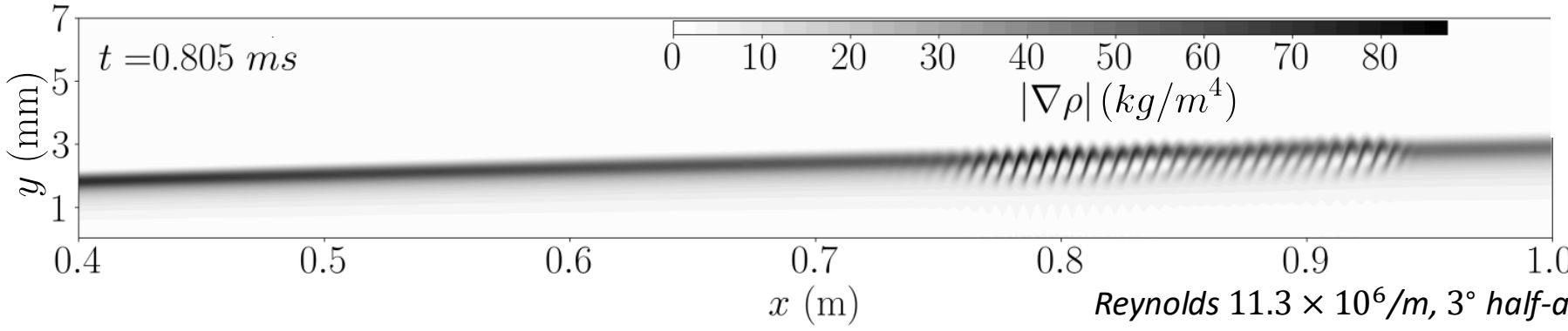

### Acoustic energy , term $iv$

Mechanical (expansion/contraction) work done on a fluid element, which gets stored as the potential energy

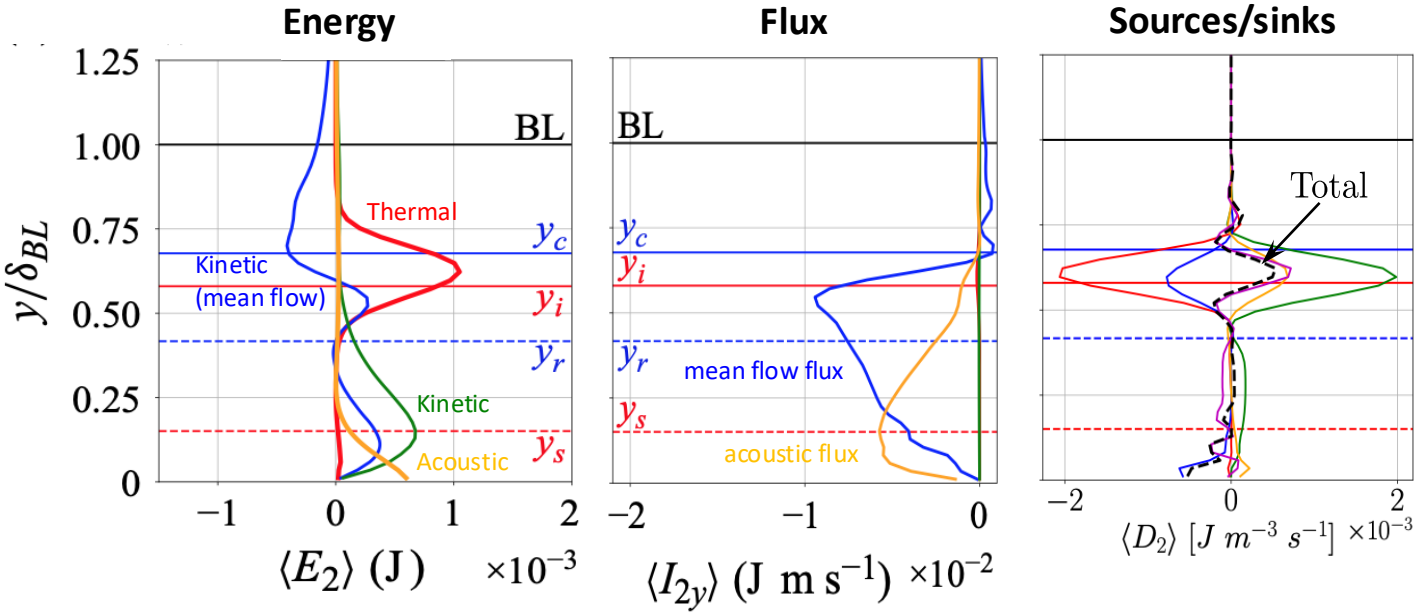



Roy, I. and Scalo, C., 2025. Disturbance energy budget of linear and nonlinear second-mode waves. *Journal of Fluid Mechanics*, *1007*, p.A49.

# Disturbance Energy Profile




*Reynolds* $11.3 \times 10^6$*/m, 3° half-angle sharp cone*




$$E_2 = E_t + E_k + E_a =$$

$$\underbrace{\frac{1}{2}\frac{\rho_0 T_0}{C_p}s'^2}_{i} + \underbrace{\rho' u_{0i} u_i'}_{ii} + \underbrace{\frac{1}{2}\rho_0 u_i'^2}_{iii} + \underbrace{\frac{1}{2}\frac{p'^2}{\gamma p_0}}_{iv}$$

Thermal energy, term $i$

Kinetic energy , term $ii + iii$

Acoustic energy , term $iv$


Roy, I. and Scalo, C., 2025. Disturbance energy budget of linear and nonlinear second-mode waves. *Journal of Fluid Mechanics*, *1007*, p.A49.

# Disturbance Energy Profile

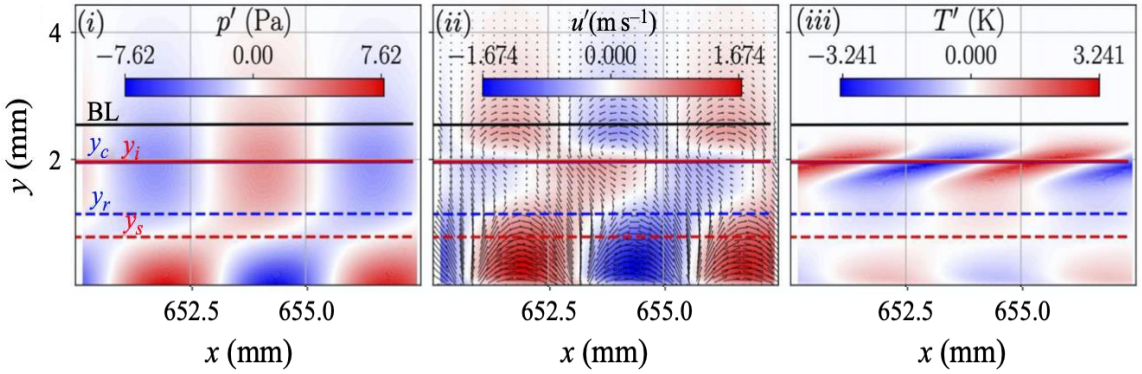
**What is the energy budget of the second-mode waves?**

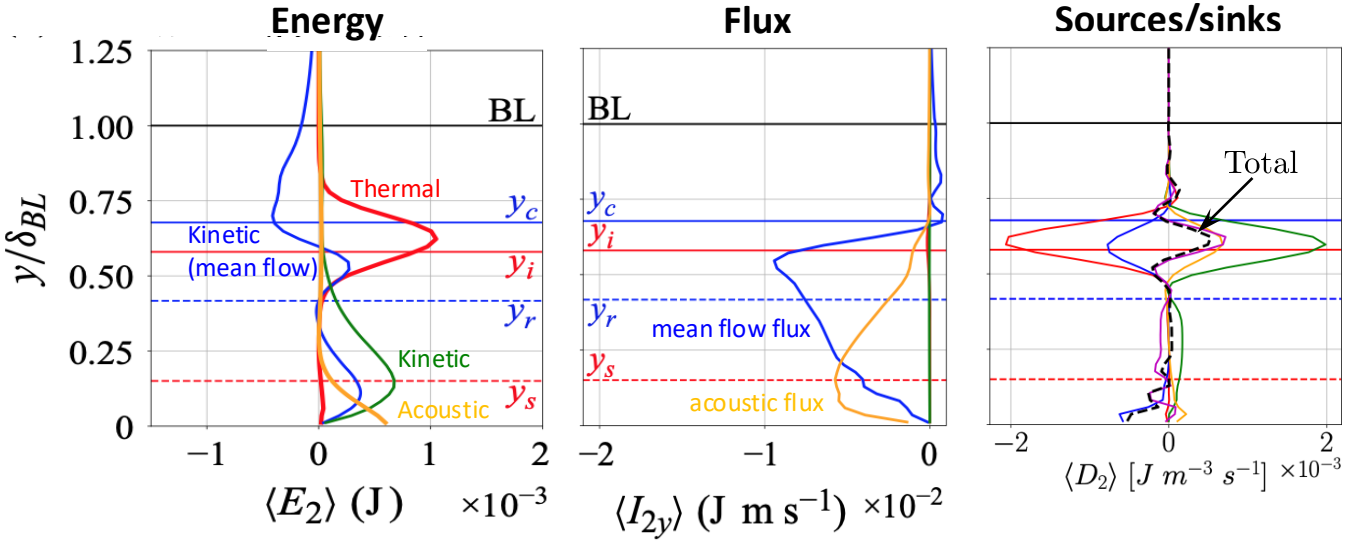
$$E_2 = E_t + E_k + E_a = \underbrace{\frac{1}{2}\frac{\rho_0 T_0}{C_p}s'^2}_{i} + \underbrace{\rho' u_{0i} u_i'}_{ii} + \underbrace{\frac{1}{2}\rho_0 u_i'^2}_{iii} + \underbrace{\frac{1}{2}\frac{p'^2}{\gamma p_0}}_{iv}$$

Thermal energy, term $i$

Kinetic energy , term $ii + iii$

Acoustic energy , term $iv$



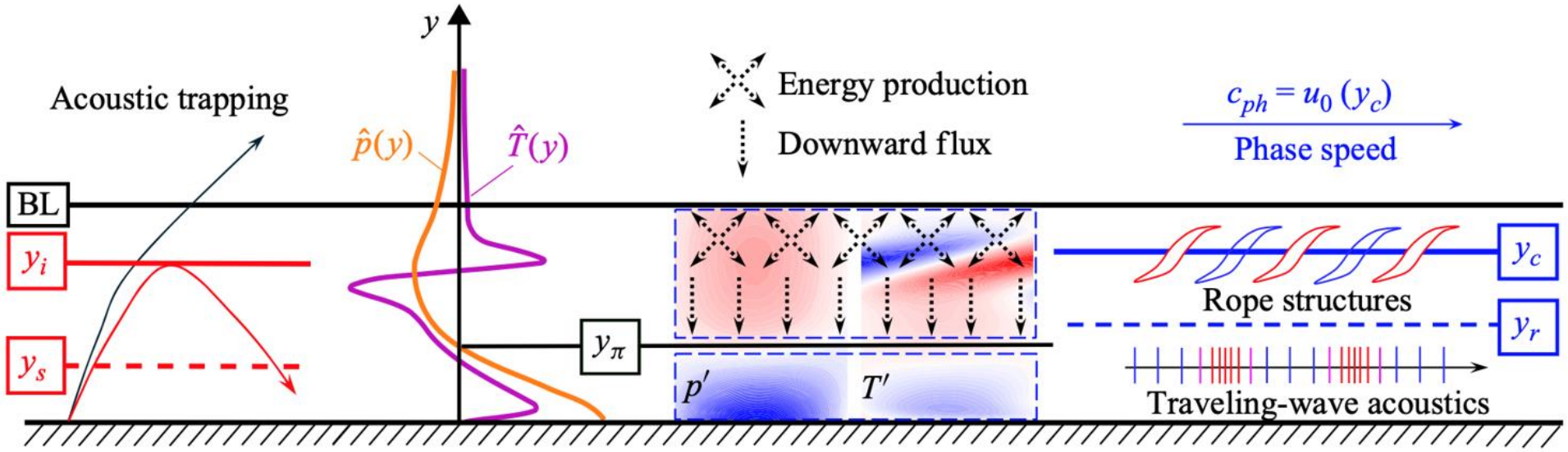



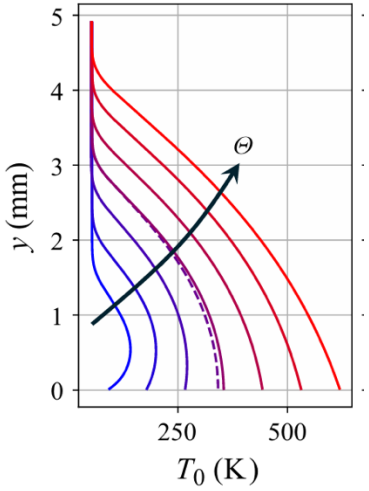

- Rather than acoustic energy (concentrated near the wall), energy content is dominated by **non-isentropic thermal dilatational energy**
- **Energy production occurs near the critical layer and is maximum at the inflection line**, caused by:
  - $\left(-\rho_0 T' v' \frac{\partial T_0}{\partial y}\right)$ → (Reynolds thermal flux)×(mean thermal gradient), thermal fluctuations transporting through a base thermal stratification normal to the cone surface
  - $\left(-\rho' u_0 v' \frac{\partial u_0}{\partial y}\right)$ → (Reynolds mass flux)×(mean shear), compressible counterpart to Reynolds stress production

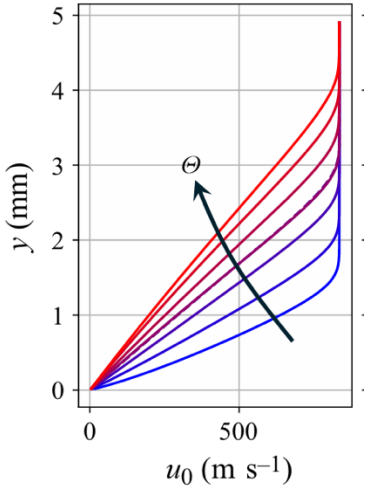

Roy, I. and Scalo, C., 2025. Disturbance energy budget of linear and nonlinear second-mode waves. *Journal of Fluid Mechanics*, *1007*, p.A49.

# Conclusion

- Transition in hypersonic boundary layers often dominated by second-mode (acoustic) instabilities
- Second mode consists of trapped acoustic waves near the wall that form a resonant structure
- Growth is highly sensitive to wall, which modifies near-wall gradients and energy transfer from the mean flow to the disturbance





Roy and C. Scalo, "Wall-temperature effects on second-mode kinematics and mechanics," Journal of Fluid Mechanics, 2026.
I. Roy and C. Scalo, "Disturbance energy budget of linear and nonlinear second-mode waves," Journal of Fluid Mechanics, 2025.
A.V. Fedorov, "Transition and stability of high-speed boundary layers," Annual Review of Fluid Mechanics, vol. 43, no. 1, pp. 79–95, 2011

# Thank you!